New Journal of Chemistry

Supporting Information

Bis(2-pyridyl)ditellane as precursor to Co^{II}, Cu^{I} and Cu^{II} complexes formation: structural characterization and photocatalytic studies

Felipe Dornelles da Silva,[a] Tanize Bortolotto,[a] Bárbara Tirloni,[a] Natália de Freitas Daudt,[b] Ernesto Schulz Lang[a] and Roberta Cargnelutti*[a]

[a.] *Department of Chemistry, Federal University of Santa Maria, Av. Roraima, n.1000, 97105-900, Santa Maria, RS, Brazil.*

[b.] *Department of Mechanical Engineering, Federal University of Santa Maria, Av. Roraima, n.1000, 97105-900, Santa Maria, RS, Brazil.*

** Corresponding author: roberta.cargnelutti@ufsm.br*

Table of Contents

Table S1. Crystallographic and structure refinement data for compounds **1**–**4**.

Compound	**1**	**2**	**3**	**4**
Formula	$C_{10}H_8N_2Cl_2CoTe_2$	$C_{10}H_8N_2Br_2CoTe_2$	$C_{20}H_{16}Br_2Cu_2N_4Te_4$	$C_{20}H_{16}Cl_4Cu_2N_4O_2Te_2$
Mw ($g \cdot mol^{-1}$)	541.22	630.13	1109.68	868.47
Crystal system	Monoclinic	Orthorhombic	Triclinic	Monoclinic
Space group	$P2_1/n$	$Pbca$	P-1	$C2/c$
a (Å)	8.4278(6)	13.9956(5)	9.5162(4)	20.7062(1)
b (Å)	12.1230(9)	15.6522(7)	9.9462(4)	8.3237(6)
c (Å)	13.7530(9)	27.3451(9)	15.3597(5)	14.6386(1)
α (°)	90	90	99.9150(1)	90
β (°)	92.779(2)	90	93.0890(1)	94.930(3)
γ (°)	90	90	108.9570(1)	90
V ($Å^3$)	1403.49(2)	5990.3(4)	1344.97(9)	2513.7(3)
Z	2	16	2	8
D_{calc} ($g \cdot cm^{-3}$)	2.561	2.795	2.740	2.295
μ (mm^{-1})	5.656	10.280	8.821	4.420
Collected reflections	31771	120581	36615	11837
Independent reflections [R_{int}]	4262 [0.0302]	7447 [0.0496]	8276 [0.0345]	2780 [0.0414]
R_1/wR_2	0.0176/0.0403	0.0379/0.0824	0.0304/0.0708	0.0414/0.0989
R_1/wR_2 (all data)	0.0190/0.0406	0.0507/0.0906	0.0452/0.0763	0.0533/0.1027
GOOF	1.254	1.079	1.028	1.209
Largest diff. peak and hole ($e.Å^{-3}$)	0.445 and -1.067	1.017 and -1.254	1.631 and -1.623	1.761 and -1.070
CCDC n°	2168607	2168608	2168609	2168610

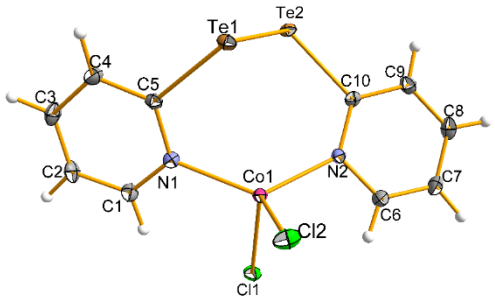

Figure S1. Thermal ellipsoid plot at the 50% probability level for the compound **1**.

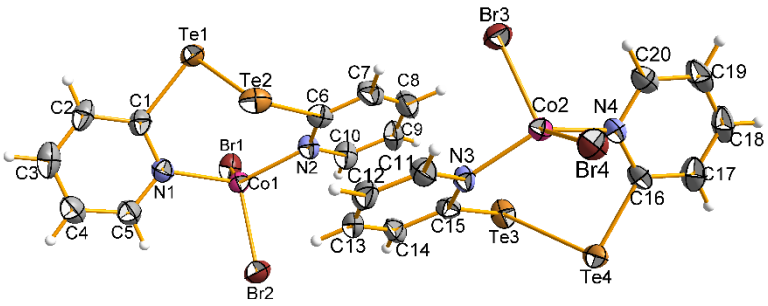

Figure S2. Thermal ellipsoid plot at the 50% probability level for the compound **2**.

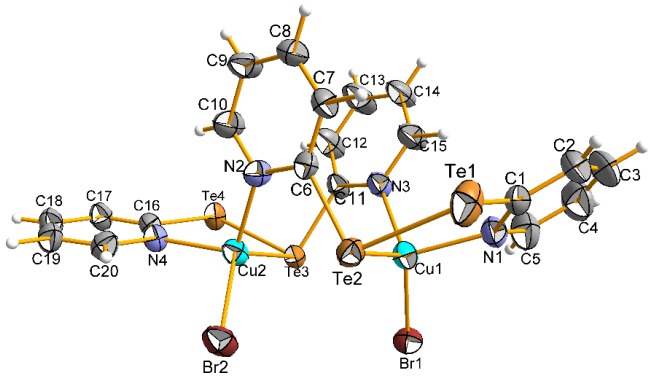

Figure S3. Thermal ellipsoid plot at the 50% probability level for the compound **3**.

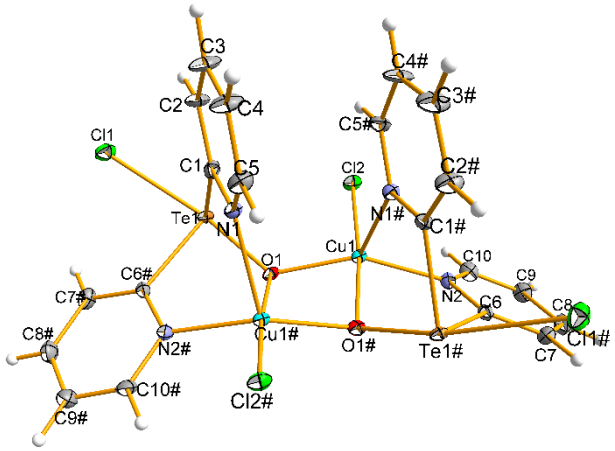

Figure S4. Thermal ellipsoid plot at the 50% probability level for the compound **4**. Symmetry code: #: $1-x, y, 1/2-z$.

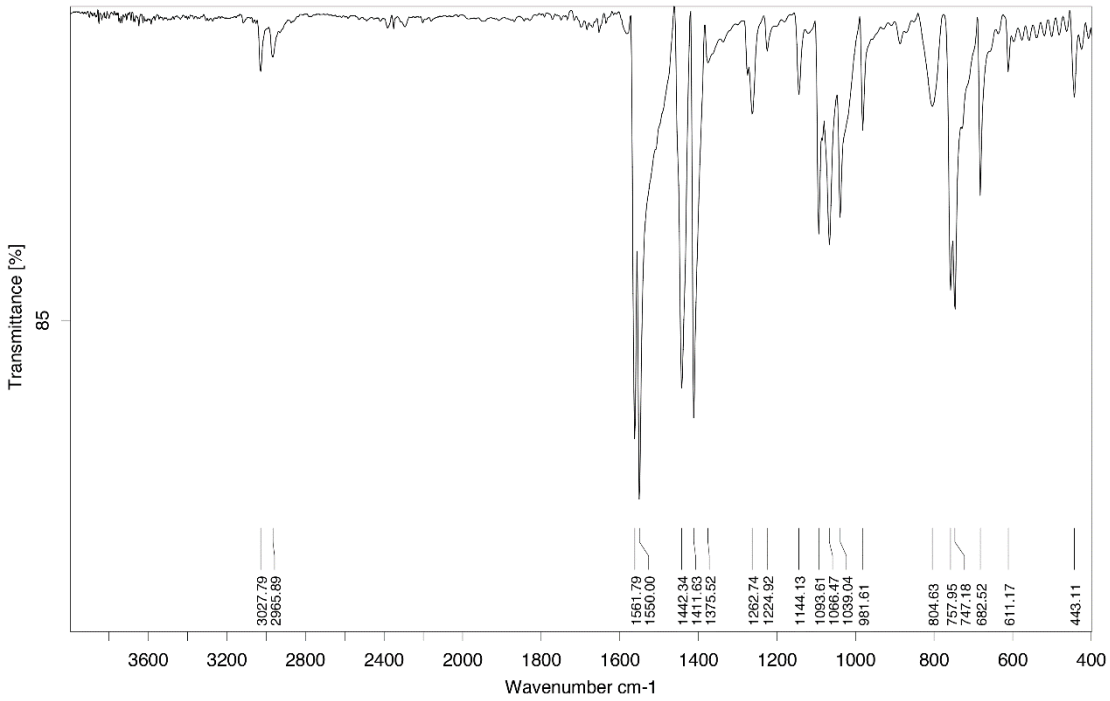

Figure S5. FT-IR spectrum of bis(2-pyridyl)ditellane $(2\text{-PyTe})_2$.

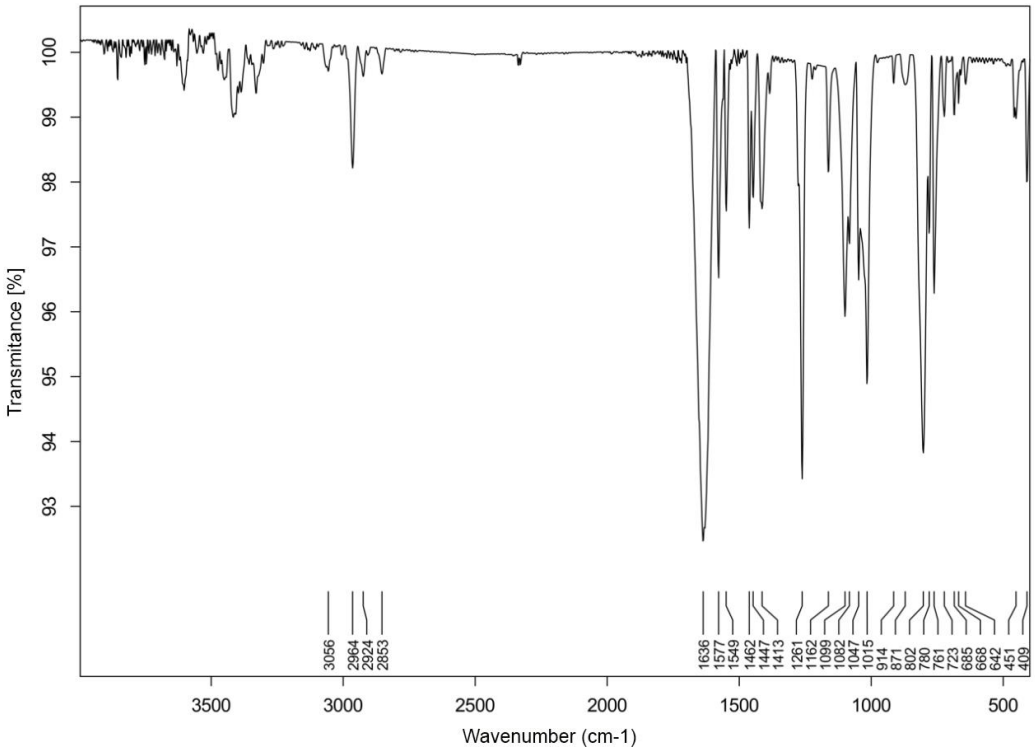

Figure S6. FT-IR spectrum of $[Co(2\text{-}Py_2Te_2\text{-}\kappa N,N')Cl_2]$ (**1**).

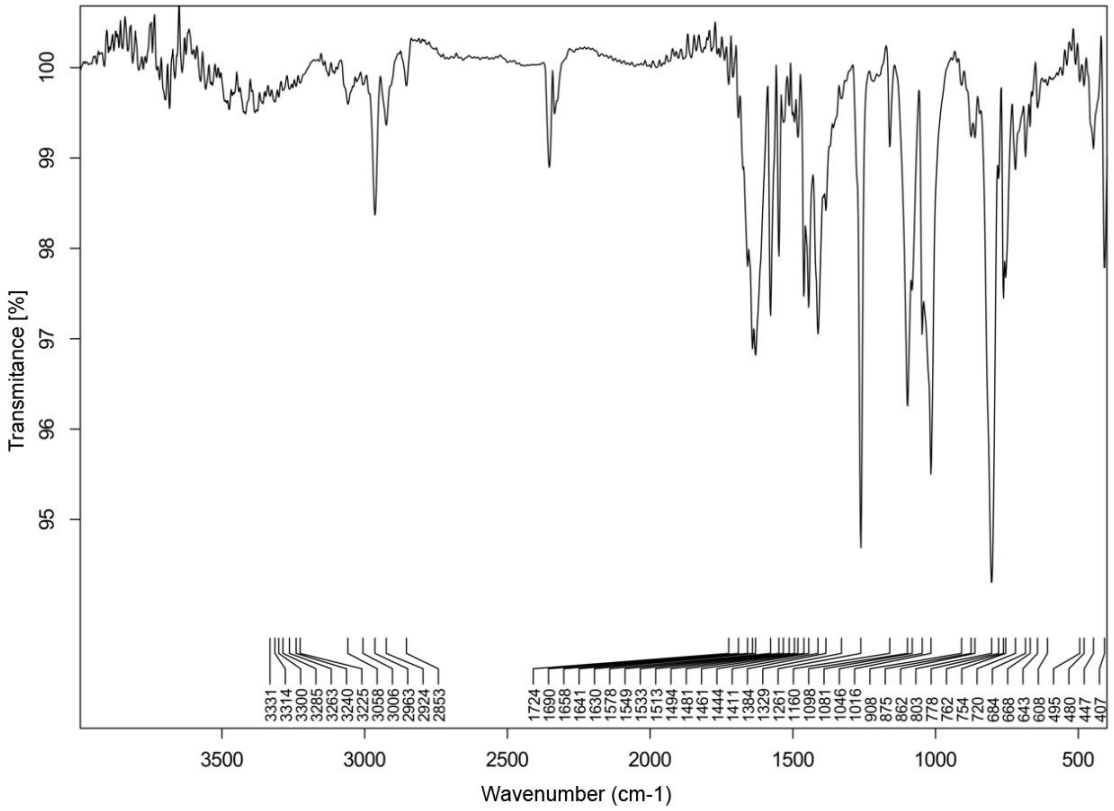

Figure S7. FT-IR spectrum of [Co(2-Py_2Te_2-κ*N,N'*)Br_2] (**2**).

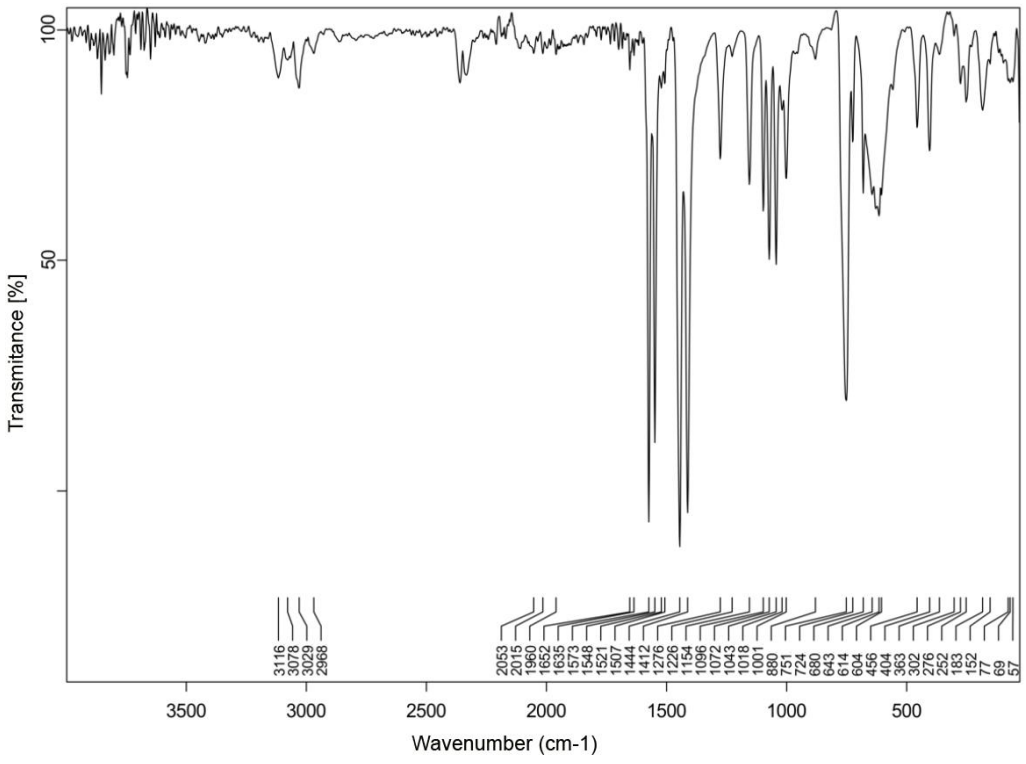

Figure S8. FT-IR spectrum of [Cu(2-Py_2Te_2-κN^1,Te^2,$N^{2'}$)Br]$_2$ (**3**).

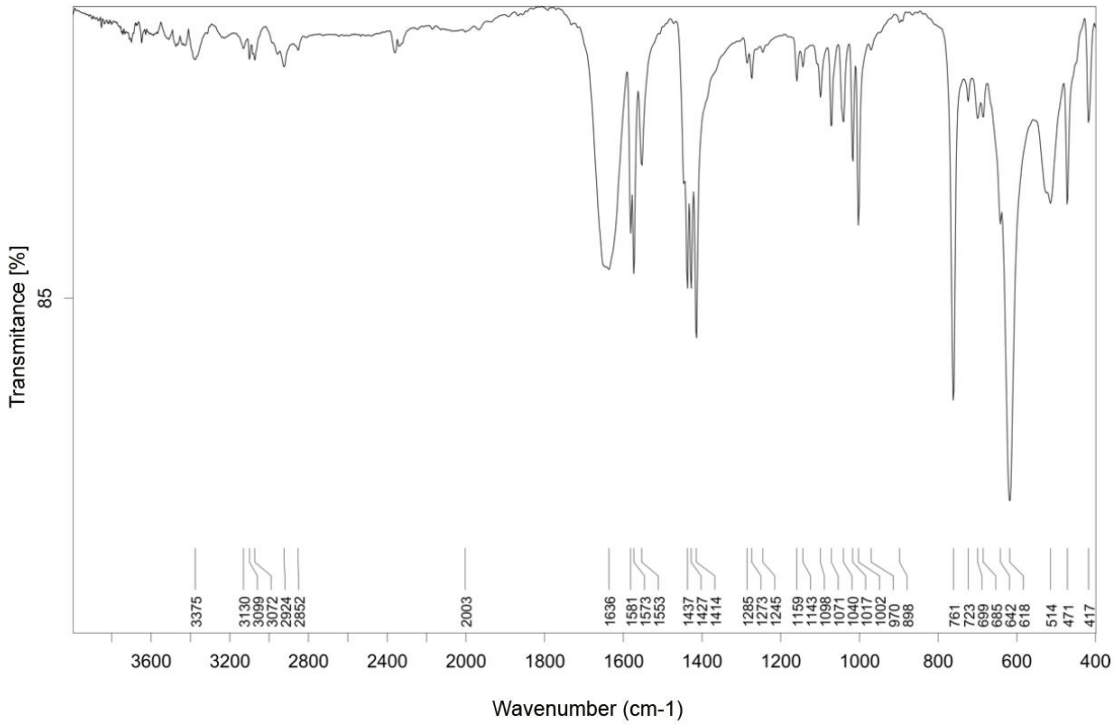

Figure S9. FT-IR spectrum of [Cu(2-Py_2TeClO-κ*O*,*N*,*N*')$Cl]_2$ (**4**).

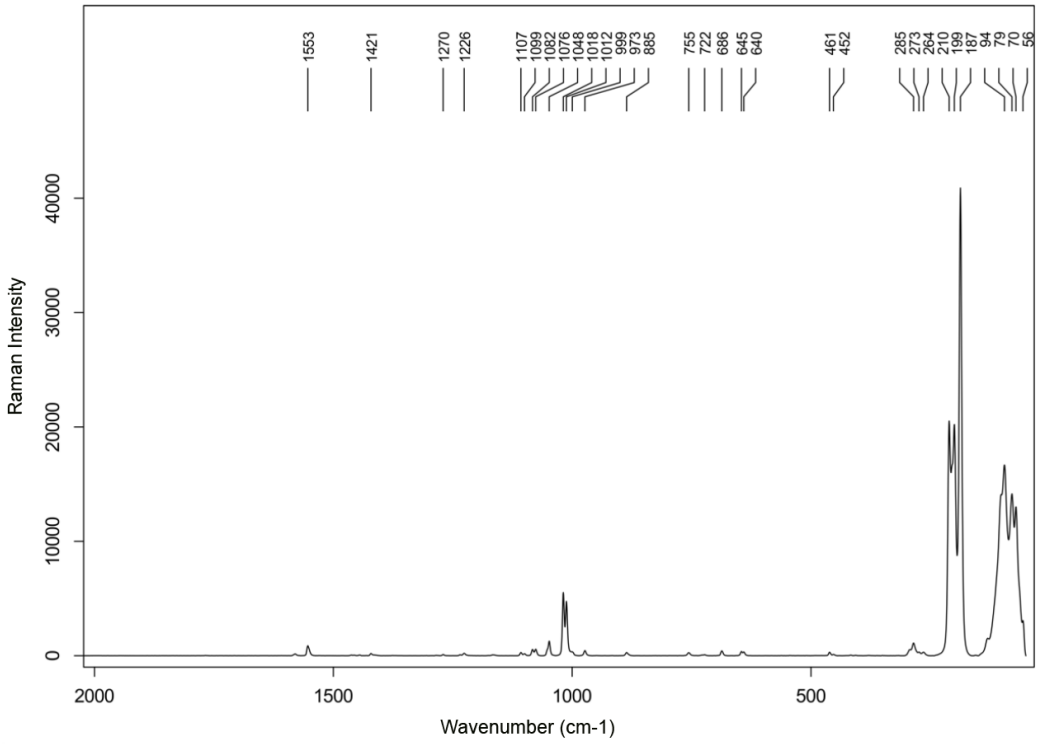

Figure S10. Raman spectrum of [Co(2-Py_2Te_2-κ*N,N*')Cl_2] (**1**).

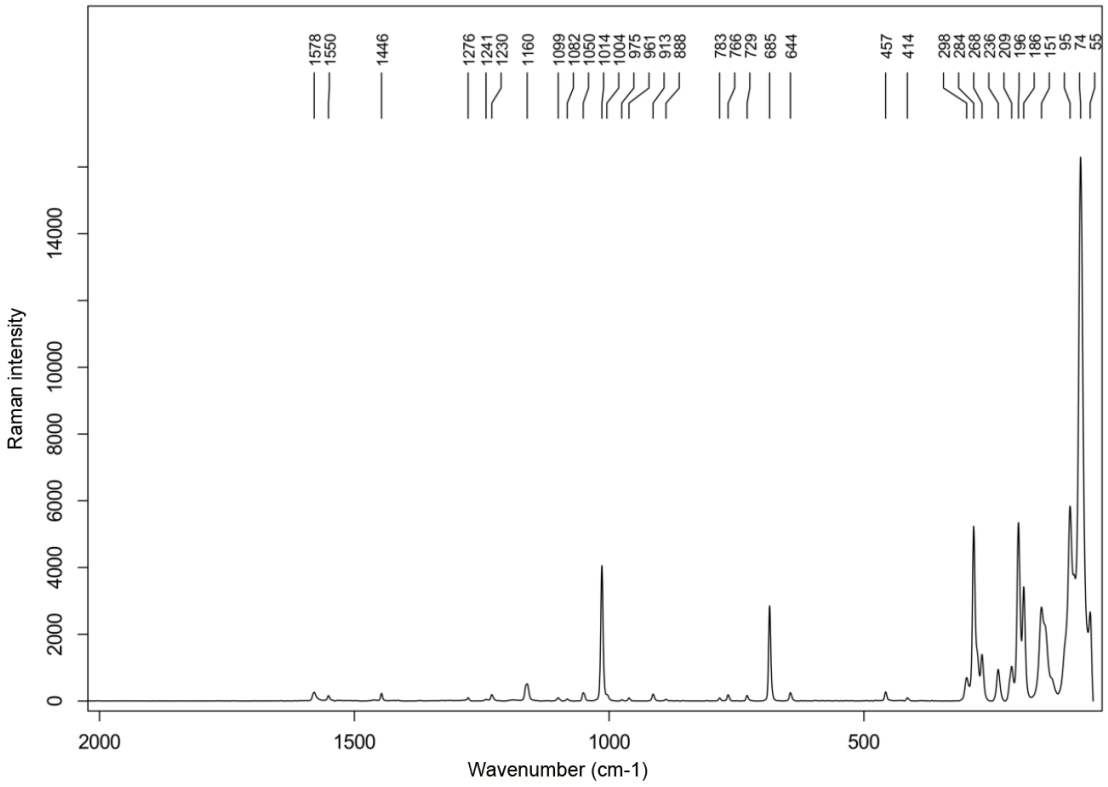

Figure S11. Raman spectrum of [Co(2-Py_2Te_2-κ*N,N'*)Br_2] (**2**).

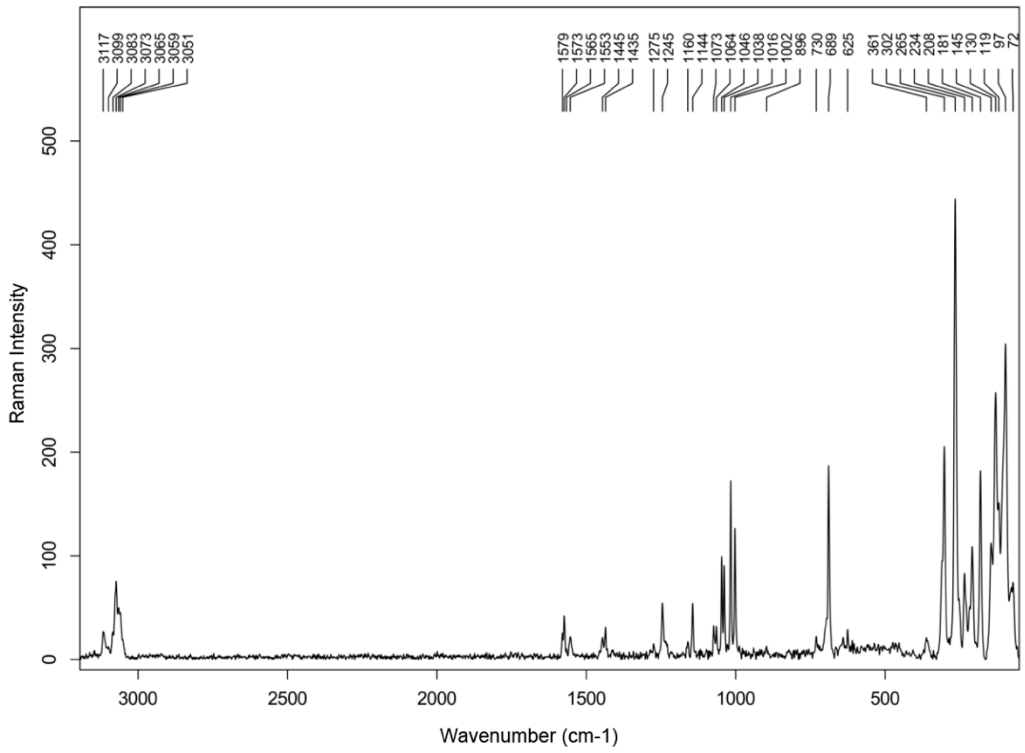

Figure S12. Raman spectrum of [Cu(2-Py_2TeClO-κ*O,N,N'*)Cl]$_2$ (**4**).

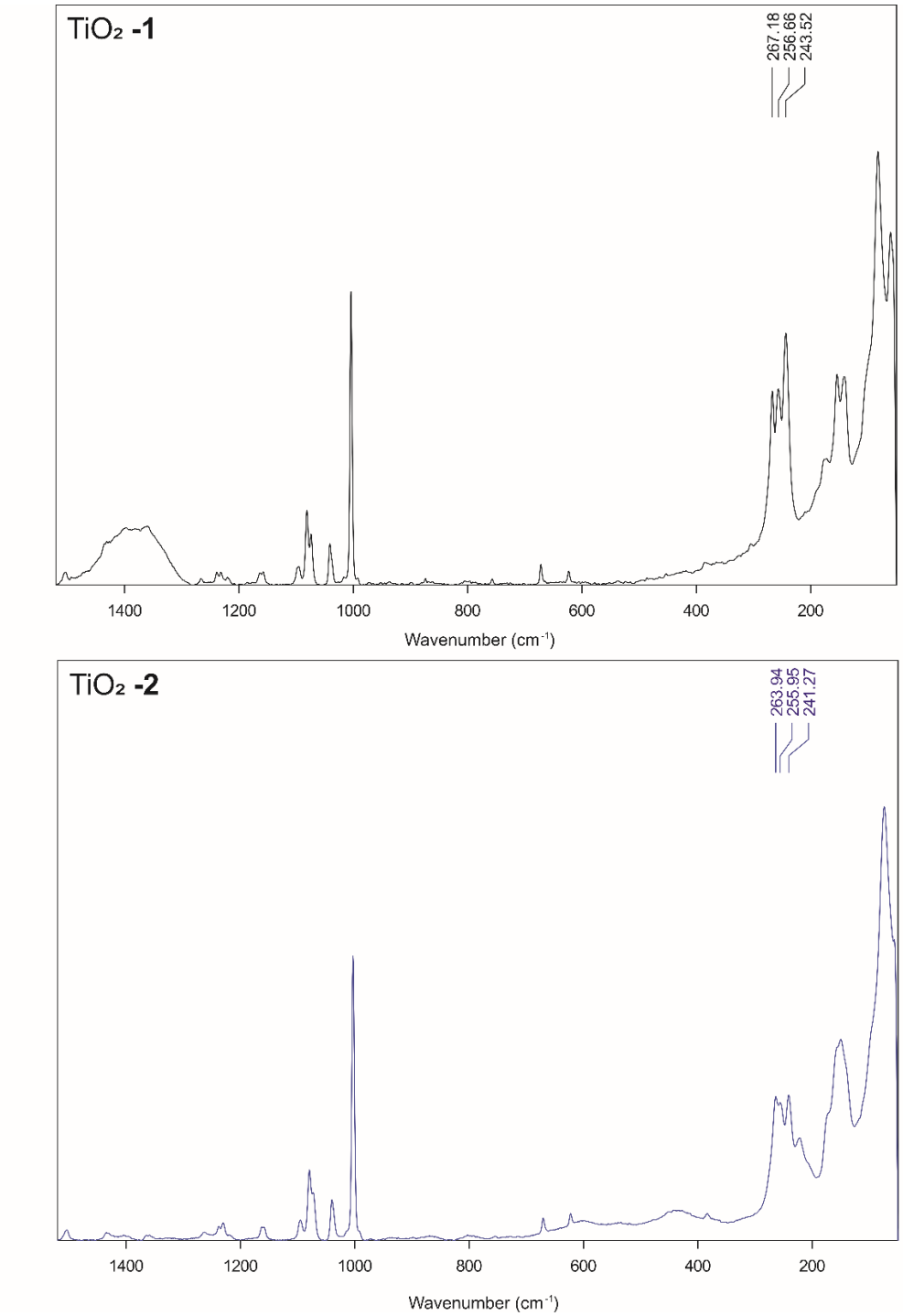

Figure S13. Raman spectra of TiO_2-**1** and TiO_2-**2**.

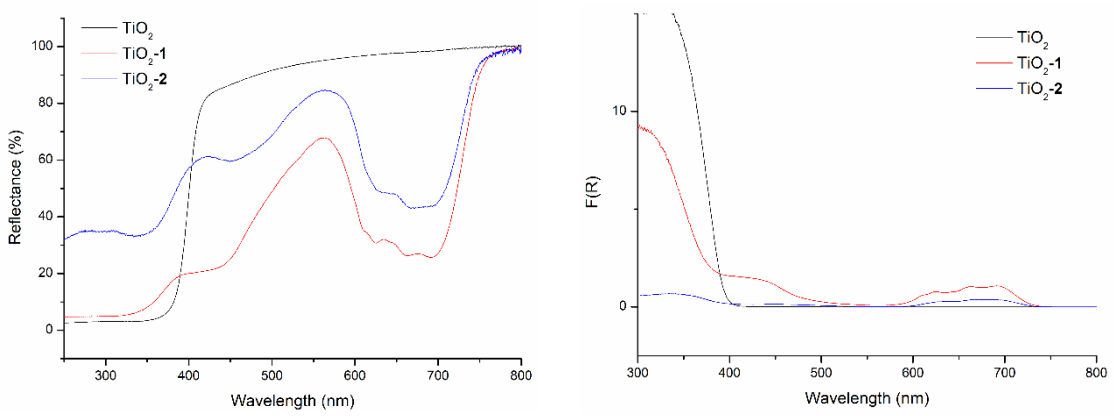

Figure S14. (a) Diffuse reflectance spectra of pure TiO_2, TiO_2-**1** and TiO_2-**2**. (b) Absorption spectra obtained from reflectance values using Kubelka-Munk equation [*F(R)* = $(1 - R)^2$ / 2R; R = reflectance][1]. For the photocatalysts TiO_2-**1** and TiO_2-**2** it was observed some absorption in the visible region of the spectra, around 450 nm and 650 nm.

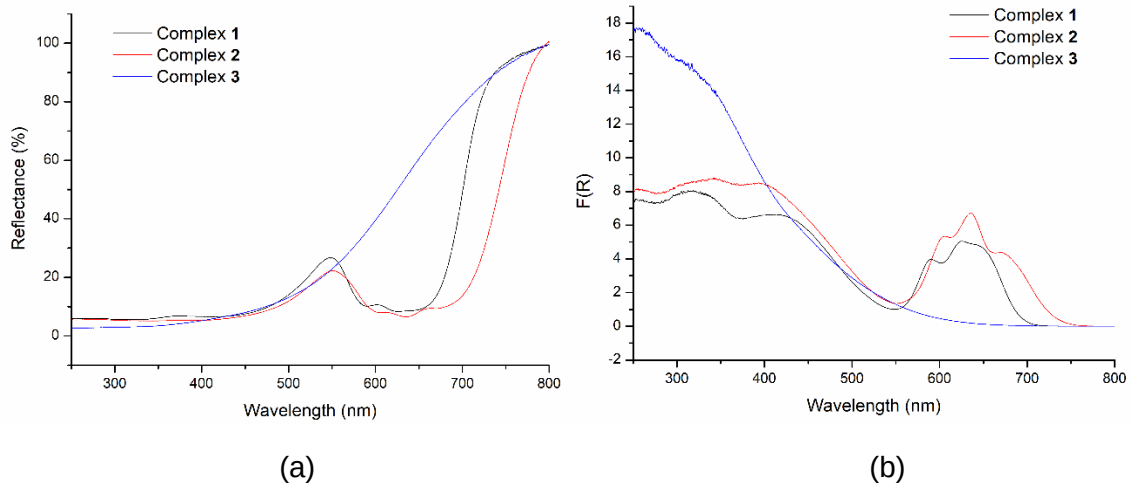

Figure S15. (a) Diffuse reflectance spectra of complexes **1**-**3**. (b) Absorption spectra obtained from reflectance values using Kubelka-Munk equation [*F(R)* = $(1 - R)^2$ / 2R; R = reflectance][1]. For the coordination compounds **1**-**3**, it was observed some absorption in the visible region of the spectra, around 400 nm and 650 nm.

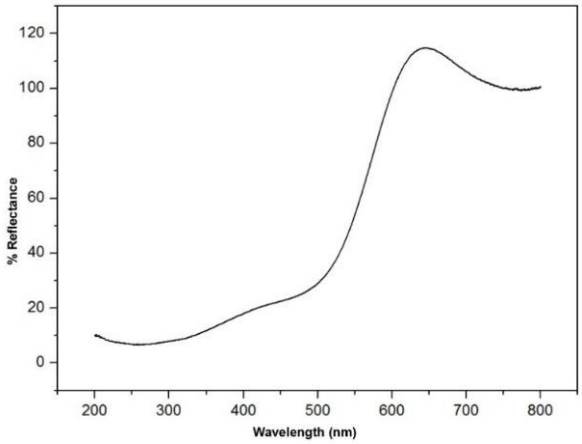

Figure S16. Diffuse reflectance spectrum of [Cu(2-Py_2TeClO-κ*O*,*N*,*N*')$Cl]_2$ (**4**).

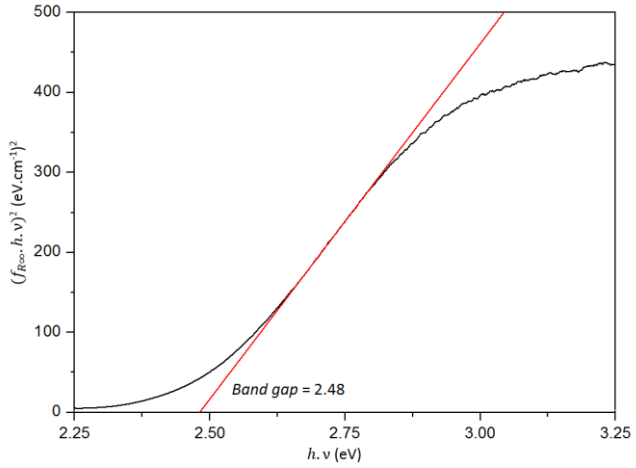

Figure 17. Graphical determination of the E_g value for [Co(2-Py_2Te_2-κ*N*,*N*')Cl_2] (**1**).

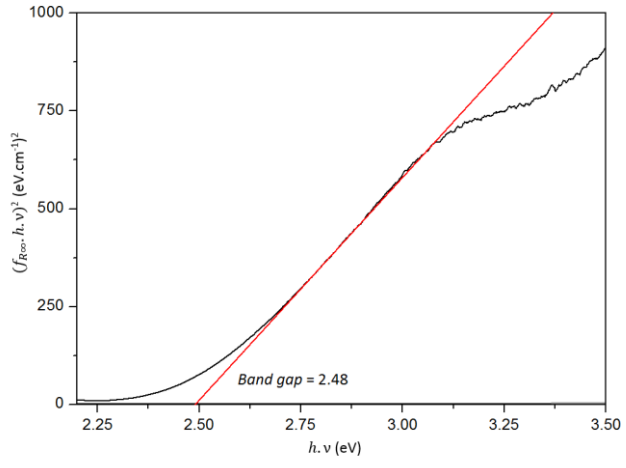

Figure S18. Graphical determination of the E_g value for [Co(2-Py_2Te_2-κ*N*,*N*')Br_2] (**2**).

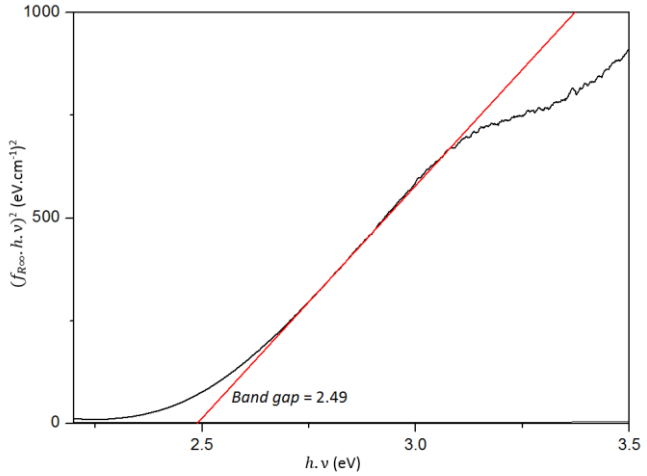

Figure S19. Graphical determination of the E_g value for [Cu(2-Py$_2$Te$_2$-κN^1,Te^2,$N^{2'}$)Br]$_2$ (**3**).

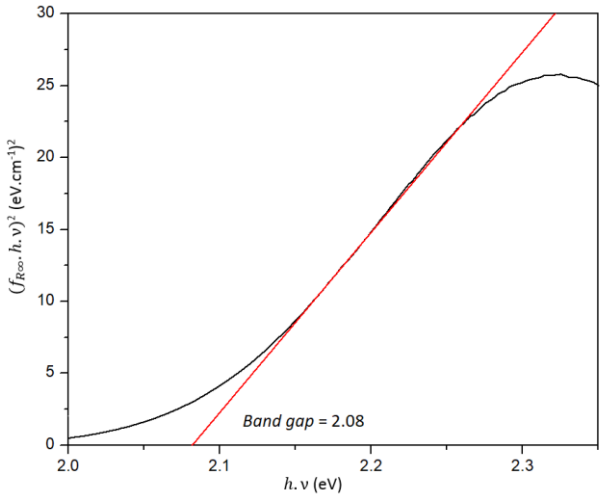

Figure S20. Graphical determination of the E_g value for [Cu(2-Py$_2$TeClO-κO,N,N')Cl]$_2$ (**4**).

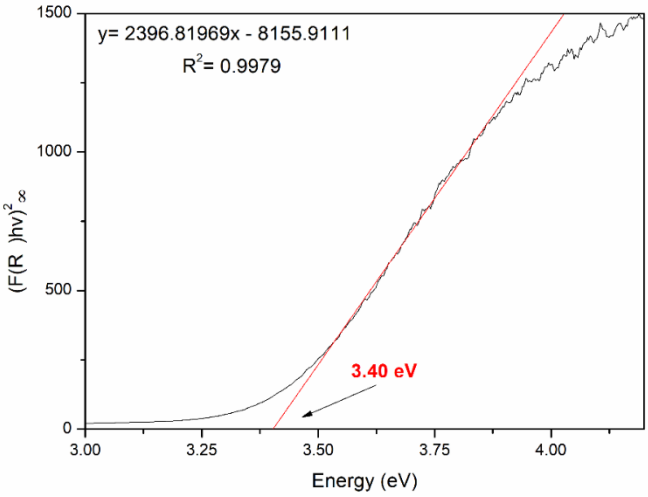

Figure S21. Graphical determination of the E_g value for TiO$_2$-**1**.

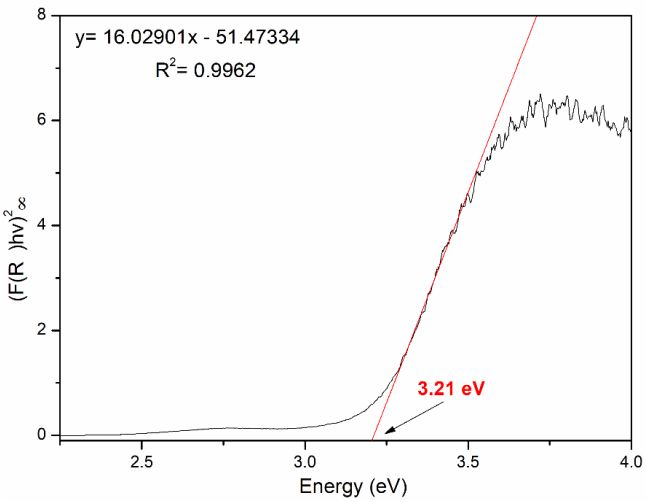

Figure S22. Graphical determination of the E_g value for TiO_2-**2**.

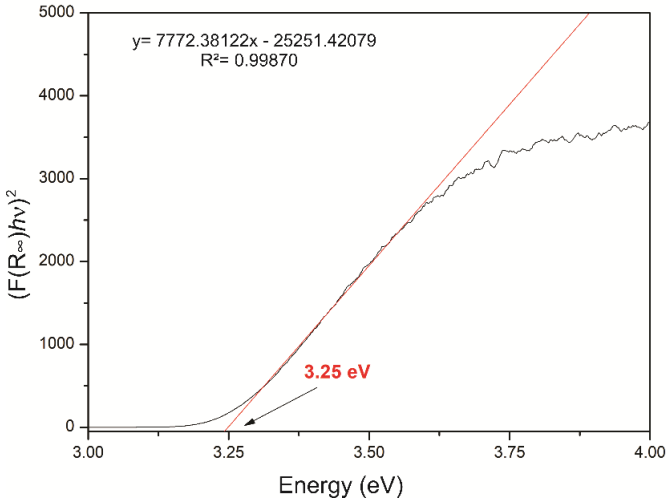

Figure S23. Graphical determination of the E_g value for pure TiO_2 synthesized by sol-gel method.

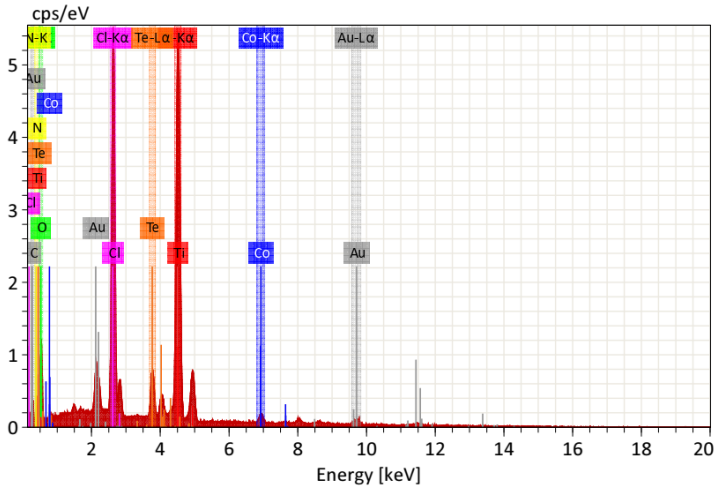

Figure S24. EDS spectrum of TiO_2-**1**. The element Au comes from metallization process.

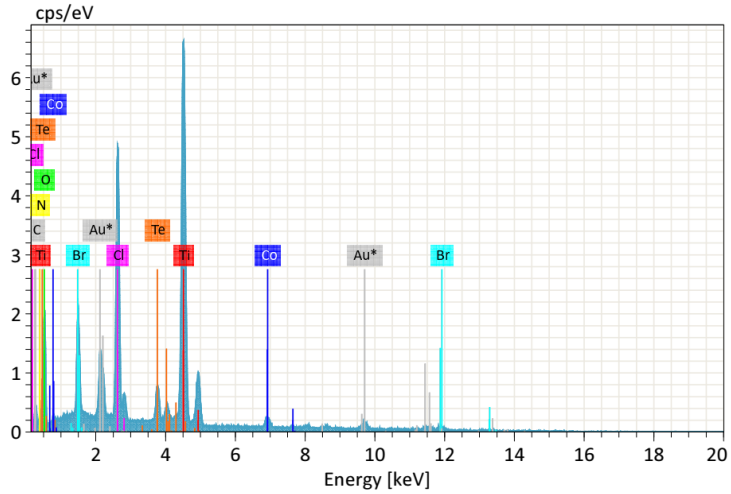

Figure S25. EDS spectrum of TiO_2-**2**. The element Au comes from metallization process.

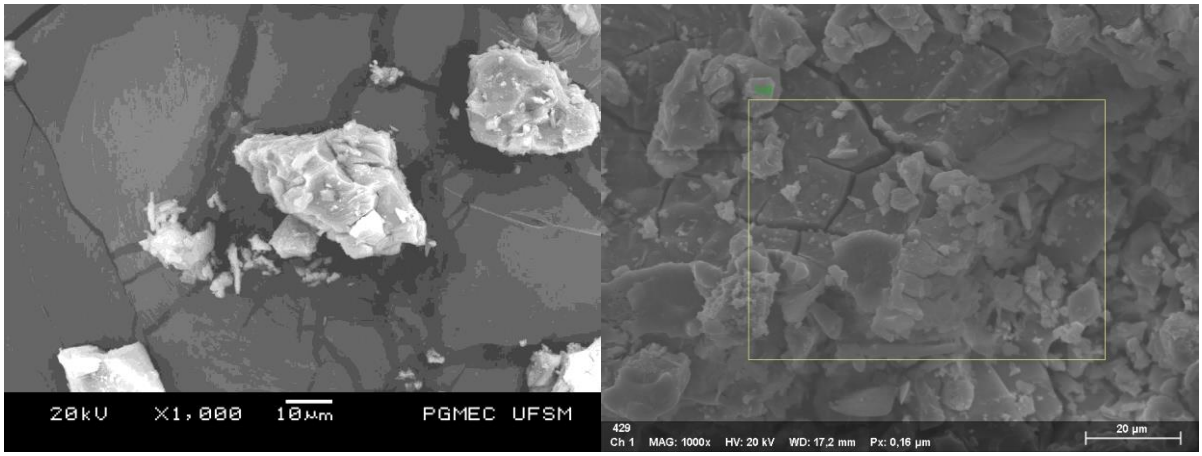

Figure S26. SEM image of TiO_2-**1**.

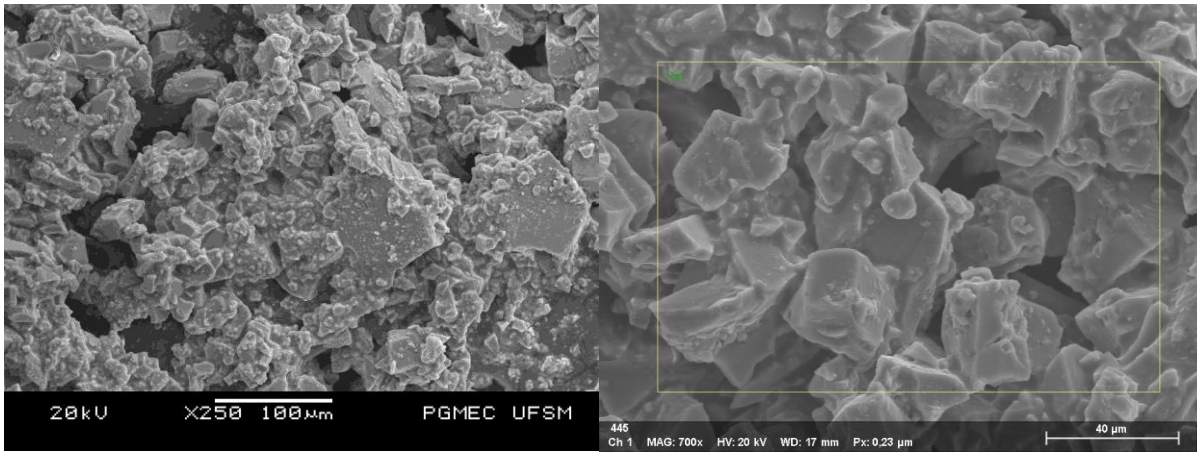

Figure S27. SEM image of TiO_2-**2**.

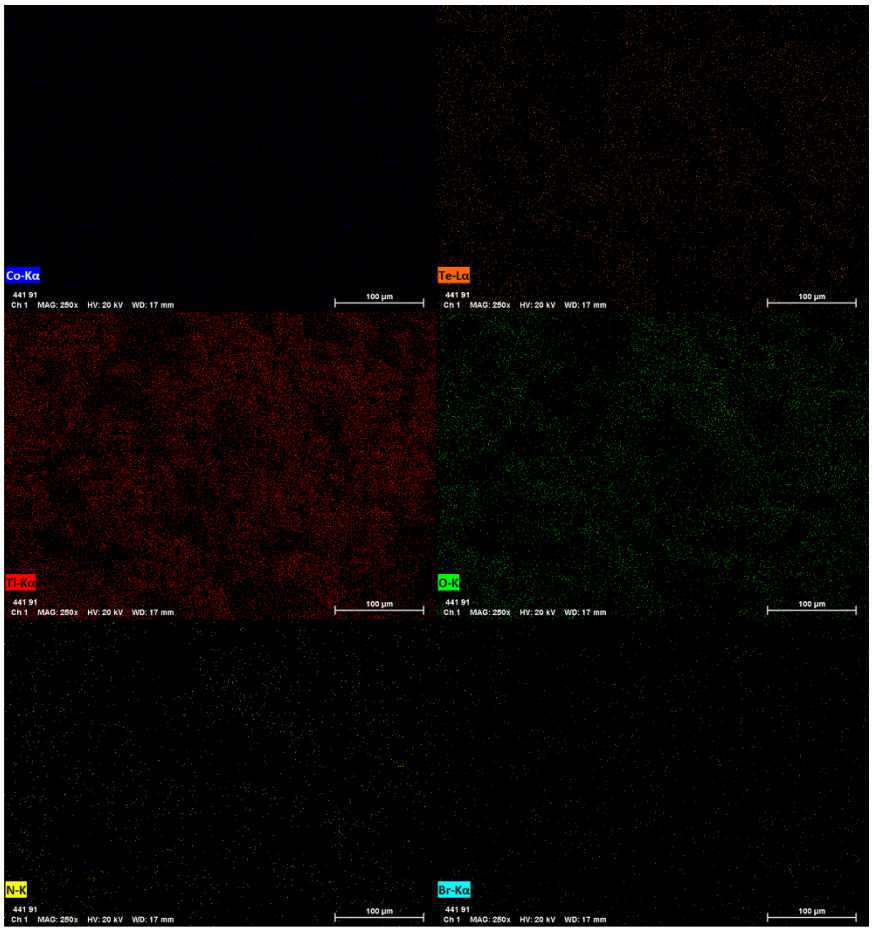

Figure S28. EDS elemental mapping images of TiO_2-**2**.

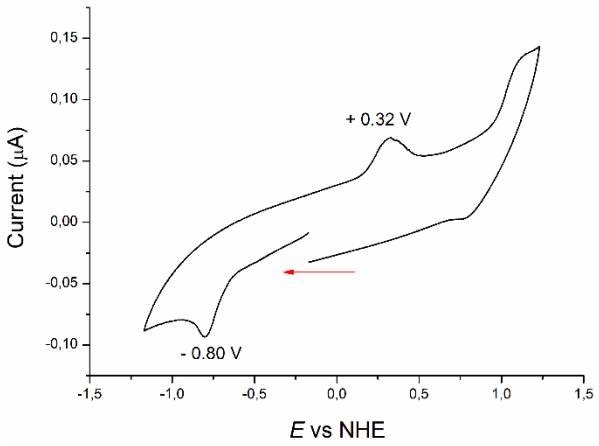

Figure S29. Cyclic voltammetry of complex **2** in CH_2Cl_2, containing 0.1 M of tetrabutylammonium hexafluorophosphate at 200 mV/s.

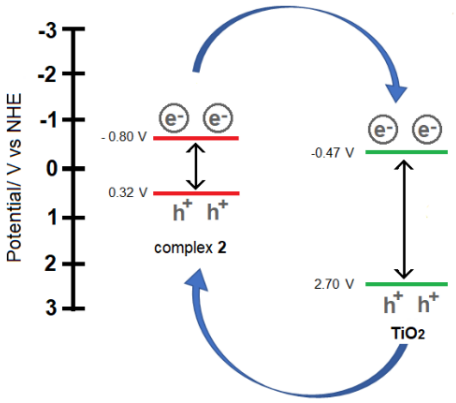

Figure S30. A schematic illustration of electron transfer from the conduction band of complex **2** to the conduction band of titanium dioxide.

Reference

[1] N. Singhal, R. Chakraborty, P. Ghosh and A. Nag, *Chem. Asian J.* 2018, **13**, 2085 – 2092.